International Journal of Education and Science Research Review
Volume-11, Issue-1 January-February-2024 E-ISSN 2348-6457
(Peer-Reviewed, Open Access, Fully Refereed International Journal) P-ISSN 2349-1817
www.ijesrr.org Impact Factor - 7.02 Email- editor@ijesrr.org

EVALUATING THE DETERMINANTS, MEASURES AND TESTING MACHINES OF STAINLESS-STEEL FATIGUE STRENGTH UNDER DYNAMIC ENVIRONMENTS

Dr. Vikram Tak

Assistant professor, Department of chemistry

S.M.P.B.J. govt college sheoganj (sirohi)

Dr. Rajender Singh

Assistant professor, Department of chemistry

govt Dungar College Bikaner

Dr. Sonlata Bargotya

Assistant Professor, Department of Chemistry

Govt. College,Tonk

ABSTRACT

Because of its resistance to corrosion and high durability, stainless steel is a material that finds widespread application in engineering applications. It is very necessary to have a solid understanding of the fatigue strength of stainless steel under dynamic conditions in order to guarantee the safety and dependability of a wide variety of structures and components. This study gives a thorough analysis of the factors, measurements, and testing machines that are utilized to determine the fatigue strength of stainless steel in dynamic situations. The first step in this investigation is to investigate the primary aspects that contribute to fatigue in stainless steel. These aspects include the material composition, the surface finish, the loading circumstances, and the environmental elements. Our goal is to get a deeper understanding of the underlying causes of fatigue failure in stainless steel by doing research on these variables and analyzing them. Following this, we will talk about a variety of methods and measurements that are often used to define and quantify the fatigue strength of stainless steel.

Keywords: *Fatigue, Test speed, Environment, Stainless steel*

INTRODUCTION

Stainless steel, of which German steel is an example, belongs to the subcategory of stainless steel known as semi-martensitic. In addition to martensite, the metal's structure also contains some ferrite in microscopic amounts. After undergoing a certain heat treatment, it possesses great strength and toughness, as well as exceptional machinability and excellent resistance to corrosion. Compressor impeller blades, cutters, and valves are some examples of the types of parts that often make use of this material because of its high level

of toughness, corrosion resistance, and impact resistance. In both local and international literature, there are very few studies on this type of stainless steel; the majority of the study focuses on heat treatment and surface properties. This type of martensitic stainless steel may be understood better with the assistance of comparative experiments on corrosion stress corrosion and corrosion of various materials used for compressor impellers.

When metal components are subjected to alternating loads, the most common type of failure that can occur is fatigue. The investigation of the characteristics of metals that are affected by fatigue may primarily be broken down into two categories: macro and micro. Experimentation and numerical modeling are used on the macroscopic level to examine the fatigue characteristics of metals and the law of crack generation and propagation. On the microscopic level, the primary focus is on researching the structure and morphological distribution of fatigue fracture. A set of regulations and criteria for fatigue failure have been defined on the basis of the two stages. The fatigue core area, the crack propagation region, and the instantaneous fracture region are the three regions that are typically present in a fatigue fracture. The primary emphasis of fatigue research is placed on determining the causes of the factors that contribute to the spread of fatigue cracks. The fatigue threshold, the overload effect, the stress ratio R, the crystal shape and grain size, and the structure are the primary elements that influence fatigue. There are many different ways to represent the growth of a fatigue fracture, and the majority of the criteria formulae are translated from semi-empirical formulas that were developed through an examination of continuous elastic-plastic deformation. The Paris formulae, which are illustrated in Formula 1, are the most fundamental examples of semi-empirical formulas. These formulas do not take into consideration influential elements like the stress ratio R. A number of different fatigue criteria models have been created in accordance with the Paris formula. These models take into account the many different aspects that might influence fatigue.

It hasn't been done very often so far, however there has been some research done on the fatigue characteristics of X12Cr13 stainless steel. After conducting in-depth research into axle fatigue, the German railway engineer Wohler came up with the idea of an S-N curve. The S-N curve not only displays the changing trend between fatigue life and stress load, but it also incorporates the process of fatigue crack initiation and propagation. This is because the S-N curve is a function of the stress-life curve. It serves as an essential foundation for fatigue design and the evaluation of the useful lives of mechanical components and technical apparatus. Internal inclusion induced failure and internal matrix induced failure are the two types of failure modes that Bomas et offered as a technique for generating a probability S-N curve for 20MnCr5 steel. Bomas et proposed this approach as a way to combine two separate types of failure modes. Using a mix of S-N curves for surface-induced fracture and internal inclusion-induced fracture, Sakai et al. examined the fatigue characteristics of a bearing steel in the long-life area under cyclic axial loading. They explained the intricate S-N behavior as a result of the combination of these two types of S-N curves. The axial fatigue behavior of spring steel 55SiCrA was investigated, the fatigue limit of the material was evaluated, and an S-N curve was constructed by Xiao and colleagues. A scanning electron microscope was used to monitor and study the shape of fatigue fractures as well as the distribution of inclusions. This allowed the researchers to determine the rule governing fatigue failure.

After doing study on the occurrence of a crack closing and opening as a result of cyclic loading, several researchers came to the opinion that a fatigue crack does not begin until after the fracture has been fully opened during the tensile section of the loading cycle. Zerbst et al. developed an analytical fracture mechanics

model for the purpose of estimating the finite life fatigue strength range of the S-N curve. This model was based on the idea that early defects, such as large second phase particles, might already have produced pre-existing fractures in the material. Experiments were conducted by Li and colleagues to investigate the effect that the quenching and tempering procedure has on the mechanical characteristics and microstructure of X12Cr13. According to the findings, both the mechanical characteristics and the structure of the material are extremely sensitive to the temperature at which it is tempered. In their research on chloride stress corrosion, Fantechi and Innocenti focused on 17-4PH stainless steel for the impeller, while X12Cr13 stainless steel served as a comparison material. When subjected to the identical conditions of the test, the stress corrosion resistance of X12Cr13 was found to be superior to that of 17-4PH. During the same time period, it was discovered that the stress corrosion resistance of X12Cr13 stainless steel is unaffected by the process of welding. Wang investigated the compatibility of austenite and ferrite in X12Cr13 stainless steel by studying their matching relationship.

In the dual-phase structure of X12Cr13 stainless steel, it was discovered that martensite makes up the majority of the material while ferrite accounts for around 40%. The hot working qualities of stainless steel are adversely affected when ferrite is present, and the plasticity of steel is drastically reduced when angular ferrite is present in the structure. Both of these effects are caused by the presence of ferrite. When Poro and Zaborski conducted research on the WEDM technology of the roots of steam turbine blades, they discovered that the structure of X12Cr13 after annealing was mostly ferrite and a little amount of carbide. However, after quenching, the structure changed into a dual-phase structure in which martensite and ferrite coexisted. After tempering, the predominant phases in the metallographic structure were pearlite and ferrite. Yan conducted research on the fatigue crack development characteristics of a variety of metals as well as the elements that impact the growth of the cracks. Based on his findings, he came to the conclusion that an increase in the stress ratio R will result in a drop in both the first crack threshold and the crack growth rate during the early stage of fatigue. Shao et al. [29] used the ANSYS finite element software to conduct an analysis of the axial fatigue characteristics of XCQ16 stainless steel. They then compared the fatigue life predicted by the simulation with the experimental data, which demonstrated the validity of the numerical analysis method in predicting the fatigue life of materials.

It is of significant reference value to investigate the fatigue fracture characteristics of X12Cr13 stainless steel and to summarize and analyze the fatigue failure law of stainless steel. This will help avoid material fatigue failure and prolong the life of the service it provides. The vast majority of current research on X12Cr13 stainless steel hasn't explicitly concentrated on the fatigue properties of X12Cr13 stainless steel, which has led to an extraordinary shortage of experimental data. This is a problem because fatigue is one of the most important characteristics of X12Cr13 stainless steel. As a result of this, the fatigue properties of the material made of X12Cr13 stainless steel were looked at in great depth during this research. The simplified lifting method was used to measure the fatigue characteristic curve (S-N curve) of X12Cr13 at R = 0.1. Additionally, the influence of the change in normal stress ratio R on the fatigue fracture characteristics of X12Cr13 was preliminarily explored in combination with the morphology analysis of the fatigue fracture surface.

Specimens and experiment procedure

X12Cr13 was the material that was investigated for this particular investigation. The fatigue test specimens were prepared in accordance with GB/T 3075-2008, and the simplified lifting technique was utilized in order to determine an estimated value for the fatigue strength of the materials. demonstrates both the fatigue test

specimens as well as the physical diagrams. Tensile testing was used to determine the real tensile strength Rm of X12Cr13 stainless steel before the fatigue testing was performed. In order to guarantee its precision, two samples were subjected to a continuous stretching process. The specimens failed with tensile force Fm of 12.3 kN, at which point they broke. The load computed value of tensile strength is determined to be 12.3 kN, and the load value for testing fatigue strength is determined to be 0.7, 0.6, 0.5...n, n-0.1 times loads. This selection was made in accordance with the criteria of the simplified lifting technique. If the number of cycles of stainless steel under a tensile load of n times is less than 107 and the number of cycles of stainless steel under a tensile stress of n-0.1 times is more than 107, then the load will be more than 107.

The American Society for Testing and Materials (ASTM) identifies the technique known as additive manufacturing (AM) as the method of fabricating three-dimensional things by superimposing successive layers of material on top of one another. Without the need for additional tooling, this technique is able to create components that have internal as well as exterior geometries that are complicated. AM has also demonstrated a great deal of promise as a manufacturing technology that has the ability to replace traditional production processes such as subtractive and joining procedures. On the other hand, additive manufacturing has not yet been fully understood and implemented; to put it another way, traditional subtractive techniques continue to account for the vast majority of the revenue generated by manufacturing businesses throughout the world.

On the one hand, additive manufacturing offers a few benefits over its competitors that use subtractive manufacturing. As an illustration, the AM procedure is often a straightforward one-step operation. In addition, it has a good influence on sustainability since it shortens supply chains, cuts down on material waste, and improves part geometries. Despite the fact that it suffers from a high specific energy consumption index (the amount of energy that is spent during the manufacturing of a material unit), it has a positive impact on sustainability. On the other hand, it does have a few drawbacks, such as the fact that it can be challenging to maintain control over the characteristics of the finished product and that it has tolerances. There are several approaches that may be taken to circumvent these constraints. For instance, Newman and colleagues proposed hybrid manufacturing as a way to merge the processes of traditional manufacturing. It is possible to profit from all of their benefits at the same time, which will allow you to minimize the impact of each of their distinct limits. The essence of additive manufacturing as a process that only requires one step is called into question by such a solution. The vast majority of these solutions are still in their infantile phases and require more study so that they may be developed.

Because the qualities of the end products of additive manufacturing are impacted by their processing history as well as several production parameters, further research is still necessary before it can be acknowledged that AM has the capacity to realize its fullest potential as a manufacturing method. As a result, one of the primary concerns of these types of studies is the development of models that can connect the microstructure, characteristics, and performance of the final products. In addition, two more noteworthy aspects of additive manufacturing are the creation of new powders and the enhancement of the quality of existing powders. In addition, one of the top focuses of research into AM is the development of a data collection of mechanical characteristics for materials that are produced by additive manufacturing. This data bank makes it easier to produce AM components with the greatest possible features by providing the necessary information.

There are various unique types of AM processes, each of which may be classified according to the production method and the energy source used. Powder feed, wire feed, and powder bed systems are the three primary

classifications that Frazier used to divide these production methods into groupings. Directed energy deposition techniques, which include powder and wire feed systems, may be utilized for manufacturing as well as maintenance. Using these methods, it is feasible to repair worn out old components by depositing fresh layers of materials on top of the existing ones. The most common use for powder bed systems is in the manufacturing industry; however, they can also be explored for use in repair and maintenance roles, albeit with less flexibility options.

Selective laser melting and SLM steels

In the additive manufacturing method known as selective laser melting, items are produced by fully melting and then solidifying successive layers of a powder material. This results in the formation of the component. This approach is distinguished from other AM processes in that it relies on a laser beam as its primary source of energy, complete melting and solidification of the powder material, and, as a final step, the application of the powder bed fusion method. These three elements form the basis of this process. An outline of the procedure is shown here in the form of a diagram.

OBJEACTIVES

1. The Study Stainless Steel Fatigue Strength, Dynamic Environments.

2. The Study Testing Machines, Determinants.

RESEARCH METHODOLOGY

For the purpose of this investigation, wires made of superelastic nitinol and stainless steel were chosen as exemplary examples of materials that are frequently found in medical implants. The diameter of the wires made of stainless steel was 0.178 millimeters, while the diameter of the wires made of nitinol was 0.500 millimeters. While the stainless steel had been exposed to 75.8% cold work, the nitinol that was supplied had been annealed. The surface of the nitinol material was given a finish that was achieved by mechanical polishing. Because of the material choices that were made, our equipment and fixtures were able to test a wide range of fatigue life, from low to high cycle fatigue. This was made possible by the material choices that were made. At room temperature and at 37 degrees Celsius in air, the two different materials were subjected to tensile testing until failure using an actuator displacement rate of 2 millimeters per minute.

The wires made of stainless steel were drawn until they broke, but the wires made of nitinol were first pulled to a strain of roughly 6%, then unloaded, and then pushed until they broke using a procedure very similar to the one described in ASTM F2516. Nitinol wires were also evaluated with digital scanning calorimetry, which was done in a manner that was comparable to that of ASTM F2004. This was done in order to determine the austenite finish temperature, Af. contains the findings of the characterisation of stainless steel, and contains the results of the characterization of nitinol. For each characterisation test, a sample size of n = 3 was utilized, and the values that were provided for strains and stresses were all engineering values. The curve shown in Figure 1 is indicative of the stress–strain relationship for each material at the various test temperatures.

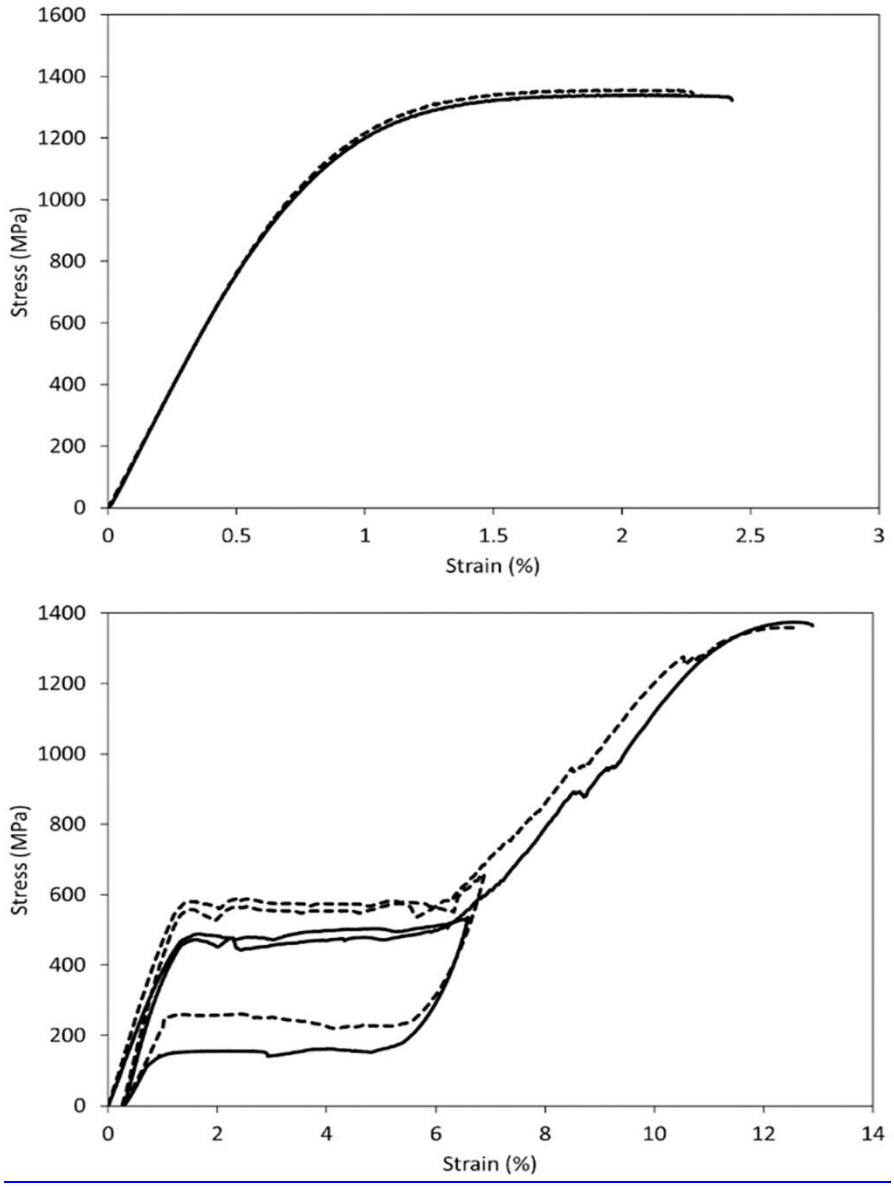

Figure 1 Representative tensile test results for the stainless steel (top) and nitinol (bottom) materials. Room temperature results are shown with a solid line and 37 °C results are shown with a dashed line.

Rotary bend fatigue

In accordance with ASTM E2948, rotary bend fatigue tests of wire were carried out in one of three environments: DIW at 37 °C, PBS (Fisher Scientific – Hampton, NH) at 37 °C, or air at ambient temperature. The PBS environment had a nominal pH of 7.4, which is similar to the pH levels that are often seen in blood. The Blockwise Engineering FTX or FTXH wire fatigue tester (located in Tempe, Arizona) was utilized throughout the duration of the tests. All of the experiments with nitinol wire were carried out in an unguided arrangement. In order to account for the possibility that heat may be generated by friction between the wire and the guides during the air testing, the stainless steel tests in DIW and PBS were carried out in a guided format, whilst the air tests were carried out in an unguided configuration.

The tests were run at speeds of either 72 revolutions per minute (1.2 Hz) or 9,000 revolutions per minute (150 Hz). The former speed was intended to simulate an approximate in vivo cardiac loading rate (72 beats per minute), and the latter speed was intended to simulate an accelerated rate that might be chosen in order to finish high cycle fatigue testing in a more reasonable amount of time. The tests at 72 RPM were carried out until either a fracture appeared or 106 cycles had been completed. On the other hand, the testing at 9,000 RPM were continued either until a fracture occurred or until 108 cycles had been completed. The alternating stresses that were applied on the wires made of stainless steel ranged anywhere from 0.3 to 0.96%. The alternating stresses that were exerted on the nitinol wires ranged anywhere from 0.6 to 2.0%. In a manner analogous to that of earlier experiments, the alternating strain, denoted by a, was calculated using the formula below, in where d represents the diameter of the wire and R represents the radius of curvature. When conducting tests on guided configurations, the radius of curvature was determined by measuring the distance between the center of the guide mandrel and the centerline of the bent wire. Analytical methods were utilized in order to determine the radius of curvature for the unguided configuration tests, as is detailed in Appendix X1 of ASTM E2948. There were a total of six wires put through their paces under each condition, including alternate strain, speed, and atmosphere, yielding a total of 180 stainless steel and 252 nitinol specimens.

Microscopy

A scanning electron microscope (SEM) manufactured by JEOL JSM-3690LV in Tokyo, Japan was used to capture images of the fracture surfaces of wires made of stainless steel and nitinol. Only a small portion of the shattered specimens could be scanned since there was such a big number of them. All speeds and conditions were photographed using the 0.68% alternating strain for stainless steel and the 0.9% alternating strain for nitinol. For those two different alternating strain situations, a representative specimen from each speed and environment condition was chosen to have a fatigue life that was close to the group average. This was done so that the specimen could serve as a benchmark for comparison. In addition, three nitinol wires that were put through an alternate strain test at 0.7% were photographed. This test was performed at 9,000 RPM. The specimens were chosen so that there would be at least one representative from each environment, as well as to cover the spectrum of fatigue life at 0.7% alternating strain. The DIW, PBS, and air samples all broke at a different number of cycles: 36,362, 29,683,979, and 99,504,792 correspondingly.

DATA ANALYSIS

Results for the fatigue life of the wires made of stainless steel may be found in. It is important to note that the coefficients for the increased test speed were computed twice. The first computation was carried out using the fatigue life data that had been suppressed at 108 cycles in accordance with the experimental procedure. Because the two test speeds had different run-out cycle counts, the second computation was carried out with the fatigue life data suppressed at 106 cycles. This was done to make it easier to make direct comparisons between the two test speeds. SEM photos of both materials, comprising images taken at every possible speed and in every imaginable situation, are exhibited in Evidence of torsional fracture may be seen in some of the fracture surfaces made of stainless steel, particularly the PBS specimens that were put through tests at 9,000 RPM. These findings are consistent with those obtained in a previous investigation, and they appear to be restricted to examinations carried out in a guided arrangement with one wire end driven and the other wire end left undriven.

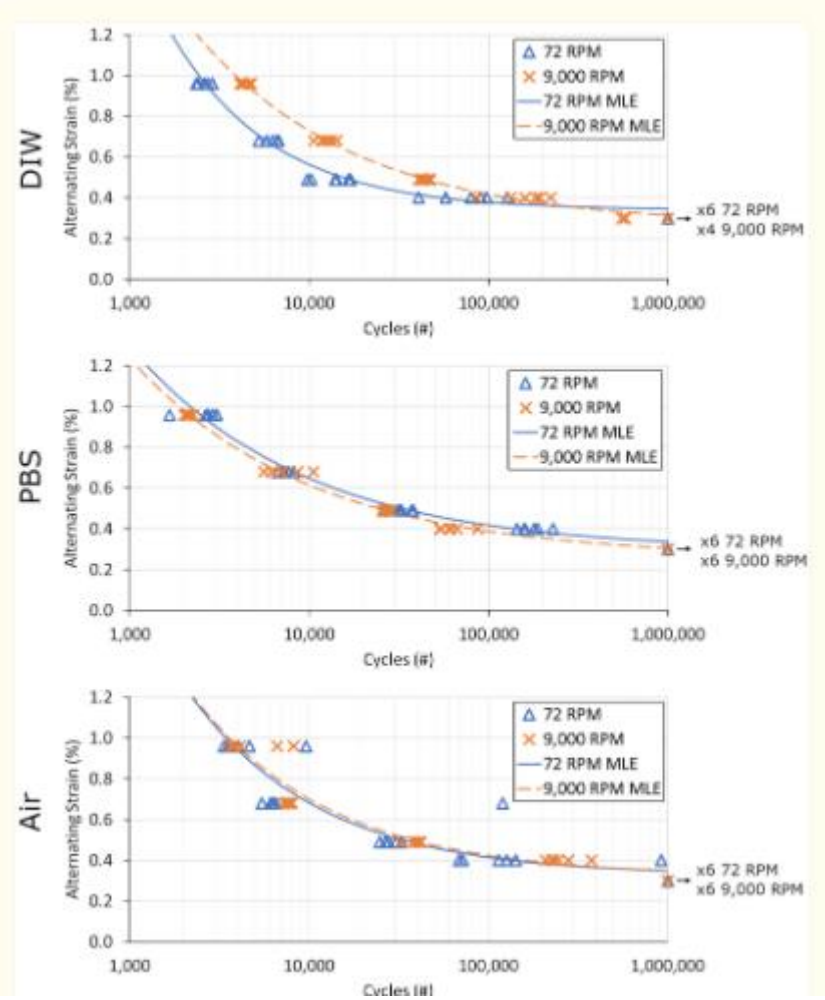

Figure 2 Stainless steel ε-N curves grouped by environment. Blue triangles represent fractures at 72 RPM and orange Xs fractures at 9,000 RPM. The solid blue line is the MLE curve for 72 RPM and the dashed orange line is the MLE curve for 9,000 RPM. Run-outs are indicated with an arrow on the right and the number of run-outs at each condition.

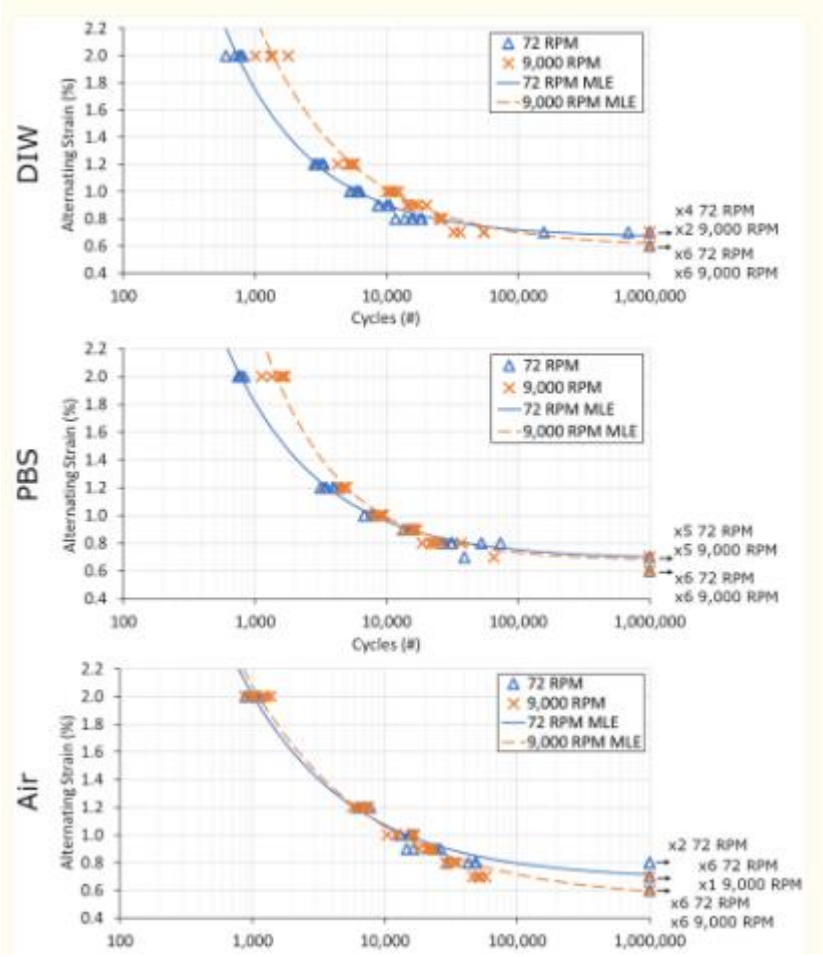

Figure 3 Nitinol E-N Curves Grouped by Environment. Blue Triangles Represent Fractures At 72 RPM And Orange Xs Fractures At 9,000 RPM. The Solid Blue Line Is The MLE Curve For 72 RPM And The Dashed Orange Line Is The MLE Curve For 9,000 RPM. Run-Outs Are Indicated with An Arrow On The Right And The Number Of Run-Outs At Each Condition.

CONCLUSION

This covers both more conventional approaches, such as S-N curves, as well as more contemporary strategies, such as finite element analysis and digital picture correlation. We evaluate the benefits and drawbacks of each strategy, and then we make recommendations for approaches that are appropriate for certain applications. In this article, we explore the testing equipment that are used to evaluate the fatigue of stainless steel, with a particular emphasis on dynamic loading circumstances. In this section, we analyze and contrast a variety of testing apparatus, such as resonance and servo-hydraulic machines, focusing on their strengths and weaknesses when it comes to imitating the dynamic situations that are seen in the real world. This study offers a detailed review of the factors, measurements, and testing equipment that are pertinent to the evaluation of the fatigue strength of stainless steel under dynamic conditions. We hope that by improving our understanding of these elements, we will be able to contribute to the creation of stainless steel-based structures and components that are safer and more dependable.

REFERENCES

1. Hurd JR, Tatum B, Grillo J, Arthurs Z, Singh N, Fong H, et al. Long-term durability of a physician-modified endovascular graft. J Vasc Surg 2020;71(2):628–34.

2. Iantorno M, Buchanan KD, Bernardo NL, Torguson R, Waksman R. Overview of the 2018 US food and drug administration circulatory system devices panel meeting on the INCRAFT AAA stent graft system. Cardiovasc Revasc Med 2019;20(5):403–8.

3. Kuo WT, Robertson SW, Odegaard JI, Hofmann LV. Complex retrieval of fractured, embedded, and penetrating inferior vena cava filters: a prospective study with histologic and electron microscopic analysis. J Vasc Interv Radiol, 2013. 24(5): p. 622–630 e1; quiz 631.

4. Marrey R, Baillargeon B, Dreher ML, Weaver JD, Nagaraja S, Rebelo N, Gong X-Y. Validating Fatigue safety factor calculation methods for cardiovascular stents. J Biomech Eng, 2018. 140(6).

5. Churchill C, Shaw J, Iadicola M. Tips and tricks for characterizing shape memory alloy wire: Part 4–thermo-mechanical coupling; 2010.

6. Wagner M, Sawaguchi T, Kausträter G, Höffken D, Eggeler G. Structural fatigue of pseudoelastic NiTi shape memory wires. Mater Sci Eng A-Structural Mater Properties Microstruct Processing 2004;378(1–2):105–9.

7. Tobushi H, Hachisuka T, Yamada S, Lin P-H. Rotating-bending fatigue of a TiNi shape-memory alloy wire. Mech Mater 1997;26(1):35–42.

8. Norwich DW. A comparison of zero mean strain rotating beam fatigue test methods for nitinol wire. J Mater Eng Perform 2014;23(7):2515–22.

9. Weaver JD, Gupta S, Woods TO. The Effects of Test Speed on Fatigue Life of Nitinol Wire in Rotary Bend. Fatigue and Fracture of Medical Metallic Materials and Devices, STP 1559, Mitchell MR, Smith Stephen W., Woods Terry, and Berg Brian T., Eds., pp. 1–17, doi: 10.1520/STP155920120213, ASTM International, West Conshohocken, PA: 2013, 2013.

10. Weaver JD, Gutierrez EJ. Comparing rotary bend wire fatigue test methods at different test speeds. J Mater Eng Perform 2015;24(12):4966–74.

11. Jerina K, Mitchell M. A precision statement for fatigue of solid round wire. J Test Eval 2018;47(4):2352–67.

12. Pelton AR, Fino-Decker J, Vien L, Bonsignore C, Saffari P, Launey M, et al. Rotary-bending fatigue characteristics of medical-grade Nitinol wire. J Mech Behav Biomed Mater 2013;27:19–32.

13. Sivan S, Di Prima M, Weaver JD. Effect of applied potential on fatigue life of electropolished nitinol wires. Shape Memory and Superelasticity 2017;3(3): 238–49.

14. Falk W A statistically rigorous fatigue strength analysis approach applied to medical devices. In: Fourth Symposium on Fatigue and Fracture of Metallic Medical Materials and Devices. 2019. ASTM International.

15. Cao H, Wu MH, Zhou F, McMeeking RM, Ritchie RO. The influence of mean strain on the high-cycle fatigue of Nitinol with application to medical devices. J Mech Phys Solids 2020;143:104057.